Corrosion Science 88 (2014) 170–177

Contents lists available at ScienceDirect

Corrosion Science

journal homepage: www.elsevier.com/locate/corsci

Kinetic properties of layer-by-layer assembled cerium zinc molybdate nanocontainers during corrosion inhibition

B.A. Bhanvase [a,*], M.A. Patel [b], S.H. Sonawane [c]

[a] Chemical Engineering Department, Laxminarayan Institute of Technology, Nagpur 440033, MS, India
[b] Chemical Engineering Department, Vishwakarma Institute of Technology, Pune 411 037, MS, India
[c] Department of Chemical Engineering, National Institute of Technology, Warangal 506004, AP, India

ARTICLE INFO

Article history:
Received 21 January 2014
Accepted 12 July 2014
Available online 21 July 2014

Keywords:
A. Mild steel
B. Modelling studies
B. TEM
B. XRD
C. Kinetic parameters

ABSTRACT

In the present study the loading of imidazole in between polyelectrolyte layers was carried out and the responsive release of imidazole was studied. Cerium zinc molybdate (CZM) was used as a core corrosion inhibitive nano pigment. The release rate of imidazole from CZM nanocontainer has been quantitatively estimated in water at different pH. The validation of quantitative analysis of release of corrosion inhibitor was carried out using the kinetic models. Results of electrochemical corrosion analysis of nanocontainer coatings on mild steel (MS) panel showed significant improvement in the anticorrosion performance of the nanocontainer/alkyd resin coatings.

1. Introduction

A problem of the modern day is rejection of materials due to corrosion which can be possibly prevented with an application of organic coatings that contain anticorrosion pigments. In recent times, numerous attempts have been focused on highly efficient corrosion inhibitive coating system with sustained release of the corrosion inhibitive agent [1]. Among the present pigments, zinc imparts anticorrosion properties by barrier and electrochemical mechanism [2]. Also molybdate conversion coatings have been investigated by many researchers as possible 'nonchromate' alternatives [3].

Technologies of encapsulation and release of various materials (e.g., drugs, oils, perfumes or corrosion inhibitors) are one of the rapidly developing research areas [4]. Nanocontainers and hollow spheres have been a subject of great scientific and industrial interest in the area of molecular biology, electronic materials, medical imaging etc. [5,6]. Furthermore, nanocontainers have been of concern to use as fillers, encapsulation of liquid agents, etc. The shells can be formed either by hydrolysis [7], in situ [8], in the presence of core materials. In the layer by layer assembly method the liquid active agent is encapsulated into the layer of oppositely charged polyelectrolyte layers. This method provides a good bonding of the organic functional groups to the metal surface, good barrier properties for corrosion protection. It is also important to note that these coatings remain active at lower temperature [9,10]. Nanopigment production using sonochemical approach is one important approach as it leads to generation of narrow size pigments with desired structures [11,12]. Following are some of the reports show the preparation of the layer by layer assembled nanocoatings. The preparation of shells on corrosion inhibitive nanoparticle that are constructed of corrosion inhibitor materials such as imidazole. To produce an inhibit impregnated polyelectrolyte shell, LbL deposition procedure involving both large polyelectrolyte molecules surrounded on inner and outer shell of the small quantity of a corrosion inhibitor has been pursued by many researchers [9,13]. Nanocontainers with a multifunctional shell can be prepared by using layer-by-layer (LbL) assembly of oppositely charged species (polyaniline and polyacrylic acid polyelectrolytes) on the surface [9]. PANI [14] is an important conducting polymer which may be used for the formation of a container because of its good environmental stability, high conductivity and low cost. It is also reported that PANI based coatings provided the protection to the metal surface against corrosive environments such as sulfuric acid solutions in the absence and presence of halide ions [15]. Kartsonakis et al. [16] have incorporated ceramic nanocontainers loaded with corrosion inhibitors into the conductive polymers coatings. The incorporation of ceramic nanocontainers loaded with corrosion inhibitor show significant enhancement in the corrosion resistance of these coatings that indicates that the presence of loaded

* Corresponding author. Tel.: +91 712 2531659.
E-mail address: bharatbhanvase@gmail.com (B.A. Bhanvase).

http://dx.doi.org/10.1016/j.corsci.2014.07.022
0010-938X/

nanocontainers into the conductive polymers coatings improved the corrosion protective properties of the films by increasing the total impedance values, and decreasing both anodic and cathodic currents relatively to coatings without nanocontainers. Kartsonakis et al. [17] also demonstrated the effect of loading of ceramic nanocontainers with corrosion inhibitor 2-mercaptobenzothiazole into hybrid organic–inorganic coatings on the corrosion protection of hot dip galvanized steel. In their report it has been reported that the corrosion resistance of these prepared coatings is found to be enhanced with loading of 4% w/w nanocontainers. Recently Kartsonakis et al. [18] have investigated the corrosion protection effectiveness of multifunctional epoxy coatings modified with pigments such as ceramic nanocontainers loaded with corrosion inhibitor, chloride and water traps, applied on AA2024-T3. Corrosion inhibitive efficiency has been reported to be improvement in the presence of the various used pigments. Saremi and Yeganeh [19] have applied mesoporous silica nanocontainer powders as corrosion inhibitor hosts and dispersed in the polypyrrole matrix. The more release of corrosion inhibitor from mesoporous silica nanocontainer has been reported at higher pHs and more aggressive chloride media indicating better protection to the substrates.

Further several kinetics models reported in the literature such as Zero order [20], first order [21], Higuchi [22], Hixson Crowell [23,24], and Korsemeyer Peppas [25] can be used to describe the corrosion inhibitor release from LbL assembled nanocontainers. These are several models available which can represent the corrosion inhibitor release as a function of time. The model equations can be derived from a theoretical analysis of the process e.g. zero order kinetics. In many cases prolonged release of corrosion inhibitor theoretical equations are not available, therefore in some case more adequate empirical equations can be used. Particle size, solubility, and types of corrosion inhibitor can influence the release kinetics. The kinetic study of the corrosion inhibitor release has been generally used to present the information about the diffusion processes and matrix degradation. Tyagi et al. [26] have studied different semi-empirical kinetic models to predict the release mechanism of benzotriazole in the solution maintained at different pH. The Korsmeyer–Peppas release model has been reported to be the best among the models used to predict the release of the corrosion inhibitor benzotriazole from silica nanocontainers.

A significant amount of work has been done in a past year, for the preparation of molybdate ion based anticorrosion coatings [11,27]. An investigation of molybdate behavior as a core material in LbL prepared nanocontainer has been not yet studied. Also it has been expected that initially release of imidazole will takes place with change in the pH of the environment which is acts as an active corrosion inhibitor in acidic as well as in basic environment and protects the substrate by the adsorption of the compact passive layer in its molecular or protonated form. Further once complete release of imidazole takes place then PANI and cerium inhibits the corrosion process thus protect the substrate from corrosion effectively [28]. With this objective in the present study CZM nanoparticles were used as a core material in the CZM nanocontainer. CZM nanocontainer was prepared by the deposition of polyaniline (PANI), imidazole and polyacrylic acid (PAA) layers on CZM nanoparticles in the presence of ultrasonic irradiation. The corrosion inhibitor (imidazole) is entrapped in between PANI and PAA layers. The responsive release and release rate of imidazole has been investigated quantitatively in aqueous media at different pH. The different theoretical and empirical equations have been used to study the release of corrosion inhibitor from LbL assembled CZM nanocontainer. The corrosion inhibition ability of CZM nanocontainer was evaluated by using dip test and electrochemical corrosion analysis method.

2. Experimental

2.1. Materials

Analytical grade zinc oxide (ZnO), cerium nitrate hexahydrate ($Ce(NO_3)_3{\cdot}6H_2O$), sodium molybdate dihydrate ($Na_2MoO_4{\cdot}2H_2O$), ammonium persulphate (APS, $(NH_4)_2S_2O_8$) as an initiator, sodium dodecyl sulfate (SDS, $NaC_{12}H_{25}SO_4$) as a surfactant and laboratory grade nitric acid (HNO_3) were procured from S.D. Fine Chem. and used as received without further purification. Analytical grade chemicals such as Myristic acid, imidazole, NaCl and methanol procured from Sigma Aldrich Chemical Co. and were used as received. Polyacrylic acid (PAA, M_w = 50,000 g mol^{-1}) was also procured from Sigma–Aldrich and were used as received. The monomer aniline (analytical grade, M/s Fluka) was distilled two times prior to use. Deionized water with conductivity of <0.2 μS/cm generated using the Elix 3 UV water purification system, has been used throughout the experimentation. Alkyd resin (Soya Alkyd Semidrying type) of Industrial grade was purchased from M/s Mahuli Paints, Pune, India. In this work Soya alkyd resin used has acid value = 06 and hydroxyl value = 56.

2.2. Preparation of cerium zinc molybdate nanocontainers

Ultrasound assisted chemical precipitation method reported by Patel et al. [11] was used for the synthesis CZM corrosion inhibitive nanopigment. Initially sodium zinc molybdate media were prepared by the chemical reaction between 0.2 M zinc oxide and 0.2 M sodium molybdate dihydrate solutions under ultrasonication. Stoichiometric amount of nitric acid was added dropwise to the above prepared mixture during the synthesis of sodium zinc molybdate media with the aid of ultrasonic irradiation. The reaction was carried out for 1 h in the presence of ultrasonic irradiation at 40 °C. Synthesis of CZM corrosion inhibitive nanopigment was carried out by chemical reaction between 0.025 M sodium zinc molybdate media and 0.016 M cerium nitrate hexahydrate solution in distilled water in presence ultrasonic irradiation for 40 min at 40 °C. The obtained precipitate was washed with hot deionized water (80–85 °C) 2–3 times in order to remove the impurity i.e. $NaNO_3$. Further, preparation of CZM nanocontainer has been implemented in a stepwise fashion. The steps are outlined here:

(1) Loading of a PANI layer onto nano CZM core by ultrasound assisted in-situ emulsion polymerization: Initially CZM nanoparticles (4 g in 150 ml water) were functionalized with 0.1 g Myristic acid solution in 5 ml methanol under ultrasonic irradiation at 60 °C for 30 min to accomplish hydrophobic properties of CZM nanoparticles. Myristic acid modification leads to adsorption of $C_{13}H_{27}COO^-$ functional group on the CZM nanoparticles surface which will create negative charge. Ultrasound assisted in-situ emulsion polymerization was used for encapsulation of treated CZM nanoparticles in PANI (positively charged) layer [15]. Encapsulation of CZM nanoparticles in PANI layer was accomplished as per below reported steps:

(i) Surfactant solution and initiator solutions were prepared separately by adding 1 g of SDS and 2 g of functionalized CZM nanoparticles (on the basis of monomer) in 100 ml deionized water and 3.5 g APS in 10 ml of deionized water respectively and then transferred to sonochemical reactor (Hielscher Ultrasonics GmbH, 22 kHz frequency 240 W power) as per method reported by Bhanvase and Sonawane [15].

(ii) In next 30 min, 5 g aniline added was in the semibatch mode in the presence of ultrasonic irradiation. The reaction was carried out for 1 h at 4 °C temperature (total reaction time 1.5 h). The formed product was separated by centrifugation (Remi Instruments Supply 220/230 V, 50 Hz, 1ϕ AC) at 8000 rpm for 10 min, and washed with deionized water to remove unreacted material and impurities. The separated PANI coated nano CZM product was dried at 60 °C in oven for 4 h.

(2) Loading of imidazole (anticorrosion agent) on PANI coated CZM: loading of imidazole layer on PANI coated CZM material (synthesized in step 1) was carried out by adding 2 g PANI loaded CZM in 0.1 N NaCl solution within 100 mL water and imidazole solution (2 mg mL^{-1}) in acidic media (pH = 3) under ultrasound assisted environment for 20 min. Further, loading of imidazole layer creates a negative charge on the surface of PANI loaded CZM nanoparticles. The obtained product was separated by centrifugation at 8000 rpm for 10 min, dried for 3 h at 60 °C and further used for loading of PAA layer.

(3) Deposition of PAA on imidazole loaded PANI–CZM Nanoparticles: to obtain responsive release of corrosion inhibitor at different pH and to make nanocontainer compatible with alkyd resin, the final PAA polyelectrolyte layer was added after the loading of imidazole on PANI encapsulated CZM nanoparticles. With the aid of ultrasonic irradiation, final deposition of negatively charged PAA layer was carried out on imidazole loaded PANI–CZM nanoparticles using 2 mg ml^{-1} PAA concentration solution again in 0.1 N NaCl for 20 min. Finally, resulting product was separated by using centrifugation at 8000 rpm for 10 min, washed with deionized water and dried in oven at 60 °C for 48 h. The formation mechanism of CZM nanocontainer is reported in Fig. 1.

2.3. Preparation of CZM nanocontainer/alkyd coatings

The coatings were prepared by dispersing CZM nanocontainers (2.0 and 5.0 wt.%) in Soya alkyd resin (total paint composition = 10 g) with a use of pigment muller (Sheen Instruments at 400 rpm). Using the bar coater desired coating thickness was accomplished (50 μm) on mild steel (MS) panels.

2.4. Characterization

XRD diffraction patterns of CZM and CZM nanocontainer were recorded by using powder X-ray diffractometer (Rigaku Mini-Flox, USA). The morphology of CZM nanocontainer was performed by using transmission electron microscopy (TEM) (Technai G20 working at 200 kV). Release of corrosion inhibitor imidazole concentration at different pH 2, 4, 7, 9 was measured using UV–vis spectrophotometer (SHIMADZU 160A model). Fourier Transform Infrared (FTIR) spectroscopic analysis of samples were carried out (SHIMADZU 8400S) in the region of 4000–400 cm^{-1}. The thermogravimetric (TGA) and differential thermal (DTA) analysis was carried using PerkinElmer TGA system (USA) from room temperature to 650 °C in N_2 atmosphere at a heating rate of 10 °C/min. The particle size distribution and Zeta potential measurements were carried out by Malvern Zetasizer Instrument (Malvern Instruments, Malvern, UK). The zeta potential measurements were carried by dispersing CZM nanocontainer in deionized water (pH = 7). The dispersion of CZM nanocontainer in alkyd coating was carried out and formed coating was applied to the MS panel (7.86 g/cm^3 density) to check its corrosion inhibition performance. The thickness of the coating film on MS plate was maintained close to 50 μm. Electrochemical corrosion analysis (Tafel plot (log |I| vs. E)) was carried out in 5% NaCl solution as an electrolyte at room temperature (25 °C) and these all characterization was performed on the computerized electrochemical analyzer (supplied by Autolab Instruments, Netherlands). Alkyd resin with three different coated MS plates containing 0, 2 and 5 wt.% CZM nanocontainer dispersed in the same alkyd resin were used as working electrode, while Pt were used as counter and Ag/AgCl as reference electrodes respectively. The area about 1 cm^2 was used for sample testing. The electrochemical window was −1.5 V to 0 V with 2 mV/s scanning rate.

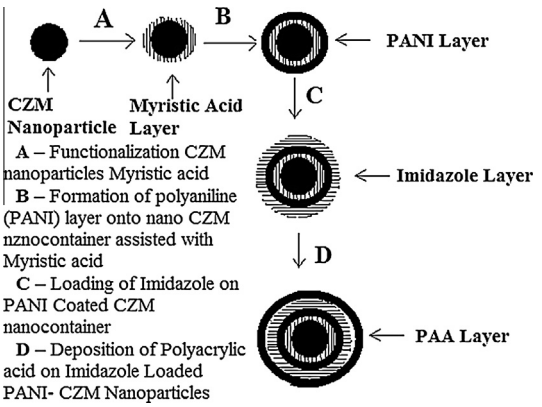

Fig. 1. Schematic illustration of the procedure for imidazole loading on CZM nanocontainer.

3. Results and discussions

3.1. Formation mechanism, particle size distribution and zeta potential of CZM nanocontainer

Fig. 1 shows the formation mechanism of CZM nanocontainer. As reported in Fig. 1, initially with a use of a novel ultrasound method synthesis of CZM nanoparticles was carried out. In the presence of ultrasonic irradiations CZM nanoparticles were functionalized with Myristic acid (MA) to improve its hydrophobicity for the compatibilization with PANI. Functionalization of CZM nanoparticles with MA leads to adsorption of negatively charged functional groups $C_{13}H_{27}COO^-$ on the surface of CZM nanoparticles. Ultrasound assisted in-situ emulsion polymerization process was used for the loading of PANI layer on functionalized CZM nanoparticles. The reduced negative surface charge is a confirmation of an adsorption of PANI layer on CZM nanoparticles. Also because of the hydrophobicity of MA coated CZM nanoparticles and developed negative charge on CZM nanoparticles, the adsorption of PANI layer is successfully taken place. Deposition of corrosion inhibitor i.e. negatively charged imidazole is achieved on PANI loaded on CZM nanoparticles. Finally deposition of negatively charged PAA layer is carried out after adsorption of imidazole layer. Use of ultrasonic irradiations during adsorption of PANI, imidazole and PAA layer results into reduced nanocontainer size which may result in uniform coating formation.

Nanocontainer stability depends upon the electrolyte strength of above mentioned adsorbed surface layers on CZM nanoparticles. Zeta (ζ) potential of the prepared CZM nanocontainer after adsorption of each layer in water is reported in Fig. 2A. The value of zeta potential of bare CZM nanoparticles is −8.13 mV. The zeta potential value is changed to −14.8 mV after functionalization of CZM nanoparticles using Myristic acid. It is attributed to the presence functional group $C_{13}H_{27}COO^-$ on the CZM nanoparticles surface due to Myristic acid adsorption. Positively charged PANI was chosen as the next layer of the MA functionalized CZM nanoparticle surface. Therefore, zeta potential value after loading of PANI layer on MA treated CZM nanoparticles was established to be −13.2 mV.

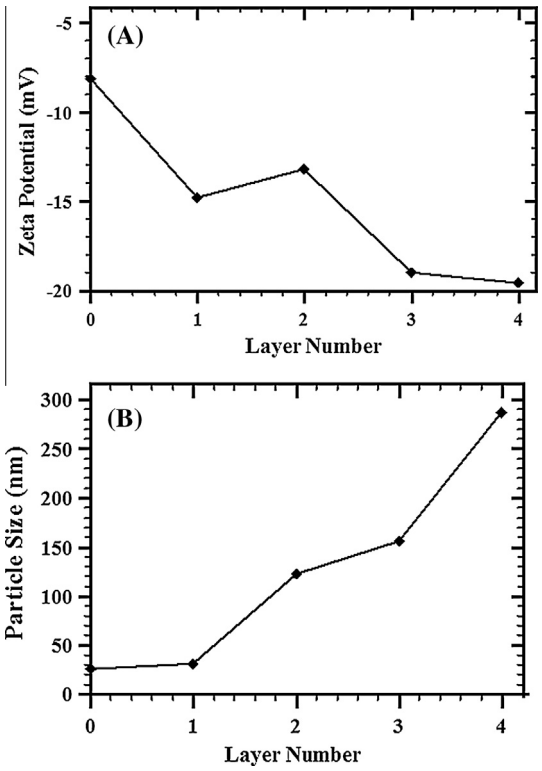

Fig. 2. (A) Zeta potential and (B) particle size of CZM nanocontainer after each layer deposition. Layer number 0: Bare CZM, 1: Modified CZM, 2: CZM/PANI, 3: CZM/PANI/imidazole, 4: CZM/PANI/imidazole/PAA.

The zeta potential after loading of corrosion inhibitor i.e. imidazole was −19.0 mV, which is attributed to the successful loading of negatively charged imidazole. After adsorption of final PAA layer, the zeta potential value again decreases to −19.6 mV. It is due to adsorption of negatively charged PAA chains. The zeta potential value confirms an intra-particle interaction and the adsorption of charged species in the CZM nanocontainer. Also the zeta potential change is reasonably small which an indication of agglomeration of prepared CZM nanocontainers. Clear agglomeration is observed in TEM images reported in subsequent section.

From the results of particle size analysis as shown in Fig. 2B, it is found that there is a formation of the layered structure of CZM nanocontainer. The initial particle size of CZM nanoparticle was established to be around 26 nm and it is found to increase to 31 nm after loading of Myristic acid layer. The formation of the PANI layer by the emulsion polymerization onto CZM nanoparticles, further, leads to increase in the particle size to 122 nm. After completion of loading of PANI onto CZM nanoparticles, the adsorption of corrosion inhibitor i.e. imidazole was carried out. Fig. 2B depicts an increase in the particle size up to 156 nm after loading of imidazole. It shows that the major imidazole was adsorbed onto the surface of PANI loaded CZM nanocontainer. Finally adsorption of PAA layer was established by emulsion polymerization onto the imidazole layer, which results in an increase in the average particle size of 287.3 nm. The average particle size is found to be increased after adsorption of each layer as shown in Fig. 2B, which indicate the successful formation of CZM nanocontainer with PANI, imidazole and PAA layers.

3.2. Morphology analysis of CZM nanocontainer

TEM images of prepared CZM nanocontainer after loading with PANI, active corrosion inhibitive agent imidazole and PAA prepared layer by layer method are depicted in Fig. 3 at different magnifications. It is found that the particle size of CZM nanocontainer prepared by ultrasound assisted method is around 110–150 nm, which is consistent with the particle size analysis as described in earlier sections. It can be ascertained from the reported TEM images that the morphology of the particles is homogeneous however some nanoparticles agglomerate due to small particle size and high surface energy [29]. The morphology of the CZM nanocontainer synthesized by ultrasound irradiation is quiet in distorted spherical shape. Further the nanocontainer particle size is smaller which can be easily explained on the basis of the effects of ultrasonic irradiation. The smaller size of CZM nanocontainers in the present work is attributed to the use of cerium zinc molybdate (CZM) nanoparticles as a template i.e. core material during preparation of CZM nanocontainers by layer-by-layer deposition of polyelectrolytes and corrosion inhibitor. CZM nanoparticles were prepared by ultrasound assisted method as per the procedure reported by Patel et al. [11]. The cavitational effects generated by the ultrasonic irradiation can result in physical and chemical transformation in the system. This improves the nucleation and solute transfer rate due to ultrasonic irradiations leads to the formation of smaller sized CZM nanoparticles. Further deposition of PANI layer on CZM nanoparticles by in-situ ultrasound assisted emulsion polymerization helps in the formation of PANI encapsulated CZM nanoparticles with average particle size of 122 nm. The deposition of imidazole and PAA has been carried out in the presence of ultrasound environment that helps in the formation of smaller size CZM nanocontainers. Further due to the presence of ultrasonic irradiation the agglomeration can be reduced to some extent leading to the formation of smaller sized CZM nanocontainers. Also in the present work agglomeration is an important issue. The main reason for getting more particle size of the CZM nanocontainer during its particle size analysis using Malvern Zetasizer Instrument

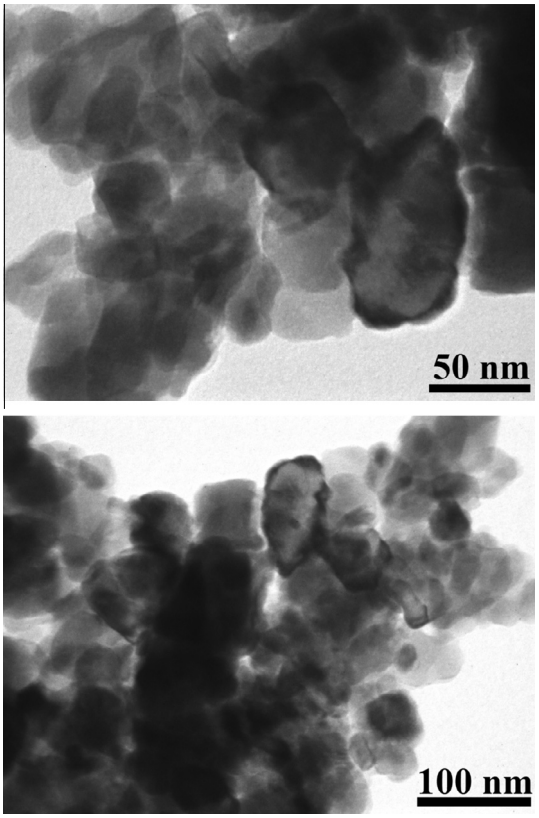

Fig. 3. TEM Images of CZM nanocontainer at different magnification.

is agglomeration of CZM nanocontainers due to its high surface energy. However maximum numbers of particles of CZM nanocontainers are fall in the particle size range of 110–150 nm which are detected in the TEM image analysis.

3.3. FTIR analysis of CZM nanocontainer

Fig. 4 depicts the FTIR spectrum of pure CZM (pattern A), Modified CZM (pattern B), CZM loaded with PANI (pattern C), CZM loaded with PANI and imidazole (pattern D) and CZM loaded with PANI–imidazole–polyacrylic acid (pattern E). FTIR spectrum of cerium zinc molybdate prepared by sonochemical method is depicted in Fig. 4 (pattern A). The characteristic peak present at 410, 727 and 833 cm^{-1} are attributed to molybdate ion [30,31]. Also the O—H stretching vibrations are depicted in region 2800–3300 cm^{-1}. The very weak characteristic peaks at 1633 and 3564 cm^{-1} is assigned to O—H stretching vibration of water molecules, due to the presence of moisture in the sample. FT-IR spectra also show characteristic peaks at 1155 cm^{-1} corresponds to Ce—O—H bending mode [32,33] and at 902 cm^{-1} corresponds to molybdate ion. Further the bands of molybdate ion and $Ce(OH)^{2+}$ in the regions of 400–800 cm^{-1} are observed which is depicted in Fig. 4A. An FTIR spectrum of Myristic acid modified CZM nanoparticle is depicted in Fig. 4 (pattern B) shows stretching vibration at 2924 and 2852 cm^{-1} in addition to the characteristic peaks of MA modified CZM nanoparticles due to C—H which came from the $—CH_3$ and $—CH_2$ in the Myristic acid respectively. Further characteristic peaks at 1400, 1468 and 1545 cm^{-1} are attributed to the bending of —OH. In this work, the FTIR spectrum of MA modified cerium zinc molybdate was obtained after eliminating the unused Myristic acid from the cerium zinc molybdate surface. In Fig. 4 (pattern C), stretching mode of an amine group (C—N) of PANI which corresponds to the characteristic peak at 1251 cm^{-1} and the peak at 1504 cm^{-1} represents a C=C stretching mode of the quinoid rings and C=C stretching of benzenoid rings respectively [34]. The FTIR spectra demonstrate that PANI layer has been coated on the surface of CZM nanoparticles. The peaks of PANI layer detected in the range between 3506 and 2995 cm^{-1} are due to the NH_2 stretching and C—H bonds, respectively [9]. Fig. 4 (pattern D) depicts the FTIR spectrum of formation imidazole loading on PANI loaded Myristic acid modified CZM nanoparticles. While in Fig. 4 (pattern D), imidazole adsorbed layer consists stretching of (C=C) bonds at 1423–1637 cm^{-1} which indicates the presence of the imidazole group in that layer [35]. Basically, imidazole is made from Myristic acid and tetramine group so in this spectrum trace of Myristic acid was also found at 2872–2937 cm^{-1}. The characteristic bands at 1749 cm^{-1} are for the PAA carbonyl C=O stretching [36].

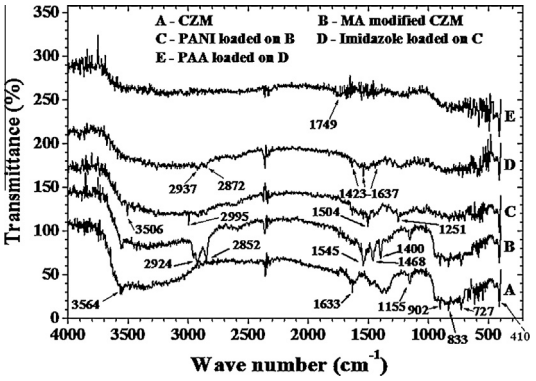

Fig. 4. FTIR spectra of: (A) bare CZM nanoparticles, (B) MA functionalized CZM nanoparticles, (C) modified CZM loaded with PANI, (D) modified CZM loaded with PANI and then imidazole and (E) modified CZM loaded with PANI, imidazole and PAA.

3.4. XRD analysis of cerium zinc molybdate nanocontainer

Fig. 5 depicts the XRD patterns of the CZM nanoparticles and CZM nanocontainers prepared by sonochemical method. XRD pattern of CZM nanoparticles is depicted in Fig. 5A. The diffraction peaks at a 2θ value of 12.2°, 14.5°, 25.2°, 26.2°, 29.2°, 32°, 34.2°, 47.7° and 48.7° are attributed to the presence of Zn, Ce and Mo oxides in cerium zinc molybdate [11,37–39] which is an indication of successful formation of cerium zinc molybdate. Fig. 5B depicts the XRD pattern of CZM nanocontainer. CZM particles were completely encapsulated with layers of polyelectrolyte and imidazole corrosion inhibitor. However, the characteristics peaks at 12.2°, 14.5°, 25.4°, and 29.4° were showing the presence of cerium zinc molybdate at the core of the CZM nanocontainer which is encapsulated in layer-by-layer assembly of CZM nanocontainer.

3.5. TGA and DTA of cerium zinc molybdate nanocontainer

Thermogravimetric analysis (TGA) curves of CZM nanoparticles and CZM nanocontainer is depicted in Fig. 6. TGA plot of CZM nanoparticles prepared by sonochemical method indicates the first weight loss (3.4%) in the range of 50–150 °C, which is attributed to desorption of free and physically adsorbed water on CZM nanoparticles [32]. The second weight loss (5.56%) in the range of 150–325 °C is due to the removal of chemisorbed water; the monolayer of H_2O molecules that directly interact with the solid surface such as cerium cations and hydroxyls; and to the dehydroxylation (release of OH^- from the structure) [33]. The total weight loss up to 700 °C is observed to be 9.6%. The possible reason behind the weight loss of CZM nanoparticles prepared by sonochemical method is due to crystallization of amorphous cerium zinc molybdate into crystalline phase [32]. According to the TG curve of the CZM nanocontainer synthesized by ultrasonic irradiation as shown in Fig. 6, the weight loss of CZM nanocontainer can be divided into three stages. The first weight loss (22.21 wt.%) is observed in the range of 50–255 °C which can be attributed to desorption of physically adsorbed as well as hydrated water in the CZM nanocontainer. The second weight loss (53.98 wt.%) is in the range of 255–485 °C can be attributed to weight loss due to burning off PAA, PANI and imidazole molecules. The third and final weight loss (3.68 wt.%) between 485 and 650 °C is due to crystallization of amorphous CZM nanoparticles. Overall, the weight loss from 255 to 485 °C is due to oxidative pyrolysis of hydrocarbon moieties present in the polymer.

The DTA curves of CZM nanoparticles and CZM nanocontainer are depicted in Fig. 7. DTA plot of CZM nanoparticles shows three

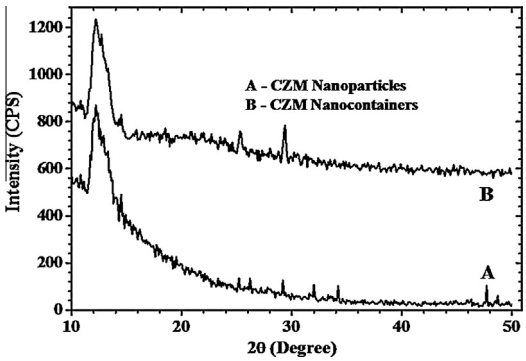

Fig. 5. XRD patterns of (a) CZM nanoparticles prepared by sonochemical method at 40 °C and (b) CZM nanocontainers.

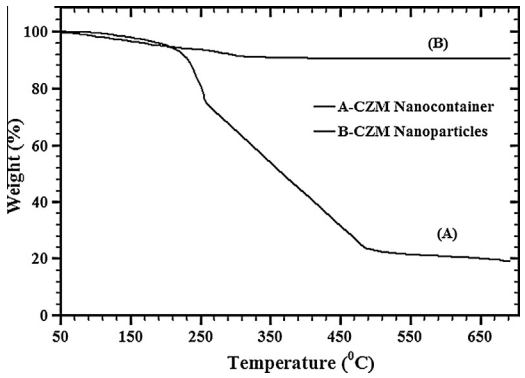

Fig. 6. TG curve of CZM nanoparticles and CZM nanocontainers in the temperature range 50–650 °C.

endothermic peaks at 180, 300 and 540 °C. The peaks at 180 and 300 °C are attributed to desorption of free and physically adsorbed water [32] and the removal of chemisorbed water (release of OH^- from the structure) [33] from CZM nanoparticles respectively. The endothermic peak at 540 °C is attributed to crystallization of amorphous cerium zinc molybdate into crystalline [32]. DTA plot of CZM nanocontainers (Fig. 7) shows endothermic peaks at 255 and 285 °C are due to removal of physically adsorbed water [32] and chemisorbed water [33] from CZM nanoparticles respectively, which in line with the discussion made in TGA section. The exothermic peaks at 425, 465 and 485 °C are attributed to multistage decomposition of PAA, imidazole and PANI respectively from CZM nanocontainer, which is well supported by TGA analysis [40].

3.6. Release study of corrosion inhibitor from cerium zinc molybdate nanocontainer

The release concentration and release rate of imidazole are depicted in Fig. 8A and B respectively. It has been found that the imidazole is a good inhibitor for ferrous metal under acidic as well as in basic environment [41–43]. Imidazole forms the compact passive layer by the adsorption of imidazole in its molecular or protonated form [44,45]. The objective of this study is to see the effect of pH of the aqueous medium (2, 4, 7 and 9) on the release of imidazole mg/g of CZM nanocontainer in 20 mL solution at different pH and on the release rate of the imidazole (mg/g of CZM nanocontainer min). It has been noted that the release of imidazole is found to be increased with respect to time then it gets stabilized, however, the release rate of imidazole increases with respect to

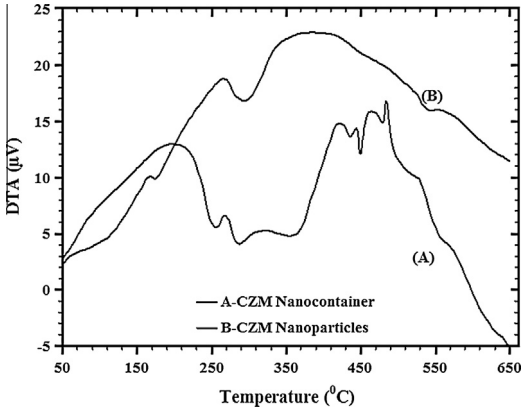

Fig. 7. DTA curve of CZM nanoparticles and CZM nanocontainers in the temperature range 50–650 °C.

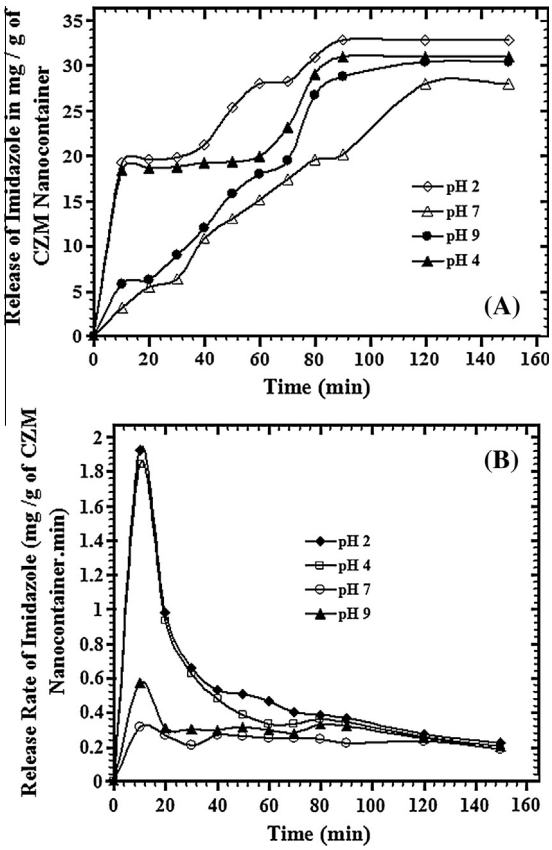

Fig. 8. (A) Release and (B) release rate of imidazole from CZM nanocontainers at different pH values.

time initially and further, it gets decreases as the concentration of imidazole increases in the surrounding aqueous medium. This increase in the release of imidazole in the surrounding aqueous medium is responsible for the decrease in the diffusion rate of the imidazole with decrease in the concentration gradient with respect to exposure time. Further it is also found that the release rate of imidazole was decreased with an increase in the pH value from 2 to 7 and again increases in basic medium i.e. at pH 9. The release rate of imidazole was found to be decreased from 1.92 to 0.31 mg/g of CZM nanocontainer min for an increase in the pH from 2 to 7 at the end of the 10 min. The larger release at pH 2 has led to the formation of passive layer of imidazole on the ferrous metal surface results in corrosion inhibition in acidic medium.

The release of imidazole was also studied using zero order, first order, Higuchi, Korsemeyer Peppas and Hixson Crowell model for different pH conditions (Table 1). Fig. 9 shows corrosion inhibitor i.e. imidazole release behavior at different pH conditions. It is found from Table 1 that the Korsemeyer Peppas and Hixson Crowell model shows better fit compared to other models [26]. Further parameter estimation has been carried out and is reported in Table 1. In all the cases, rate constant values are found to be more at pH 2 and pH 9 compared to pH 7 indicating more diffusion of corrosion inhibitor in acidic and basic condition giving better corrosion inhibition performance [46,47].

3.7. Electrochemical characterization of CZM nanocontainer/alkyd coatings

Fig. 10 depicts the electrochemical analysis (Tafel plot) for neat alkyd resin coatings, and coatings with 2 and 5 wt.% loading of CZM nanocontainer in alkyd resin and then coated on MS panel, which

Table 1
Model equations details and its comparison for release of corrosion inhibitor from CZM nanocontainer.

pH	Zero order $Q_t = Q_0 + k_0 t$		First order $\ln(M_\infty/M_t) = kt$		Higuchi model $Q_t = K_H t^{1/2}$		Korsemeyer Peppas $Q_t/Q_0 = k_t t^n$			Hixson Crowell $W_0^{1/3} - W_t^{1/3} = \kappa t$	
	k_0 (mg of Imidazole/g of CZM nanocontainer min)	R^2	k (min^{-1})	R^2	K_H (mg of Imidazole/g of CZM nanocontainer $min^{1/2}$)	R^2	k_t (min^{-n})	n	R^2	κ (mg of $Imidazole^{1/3}$/g of CZM $nanocontainer^{1/3}$ min)	R^2
2	0.46	0.36	0.038	0.91	3.606	0.876	0.000603	0.24	0.79	0.033	0.85
7	0.25	0.99	0.016	0.99	1.853	0.879	0.000026	0.91	0.98	0.014	0.98
9	0.31	0.97	0.027	0.79	2.291	0.860	0.000052	0.76	0.92	0.020	0.90

Q_t = amount of corrosion inhibitor (mg of Imidazole/g of CZM nanocontainer) released in time t, Q_0 = initial amount of corrosion inhibitor (mg of Imidazole/g of CZM nanocontainer) in the solution (in this case $Q_0 = 0$), k_0 = zero order release constant (mg of Imidazole/g of CZM nanocontainer min), M_t = corrosion inhibitor present in CZM nanocontainer (mg of Imidazole/g of CZM nanocontainer) at time t, M_∞ = Initial amount of corrosion inhibitor in CZM nanocontainer (mg of Imidazole/g of CZM nanocontainer), k = first order rate constant (min^{-1}), K_H = Higuchi dissolution constant (mg of Imidazole/g of CZM nanocontainer $min^{1/2}$), W_t = remaining amount of corrosion inhibitor in CZM nanocontainer (mg of Imidazole/g of CZM nanocontainer) at time t, W_0 = Initial amount of corrosion inhibitor in CZM nanocontainer (mg of Imidazole/g of CZM nanocontainer), κ (kappa) = constant incorporating the surface-volume relation (mg of $Imidazole^{1/3}$/g of CZM $nanocontainer^{1/3}$ min), k_t = Release rate constant (min^{-n}), n = release exponent.

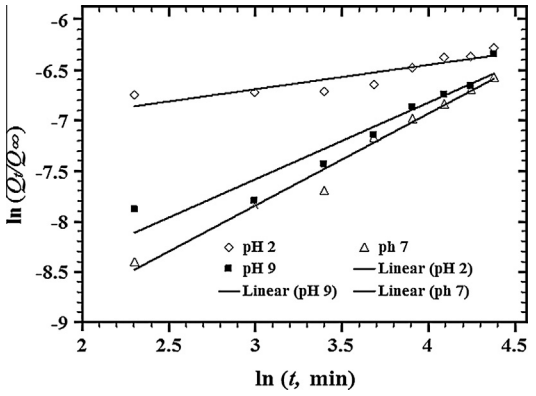

Fig. 9. Corrosion inhibitor (imidazole) release behavior using Korsemeyer Peppas model for different pH conditions.

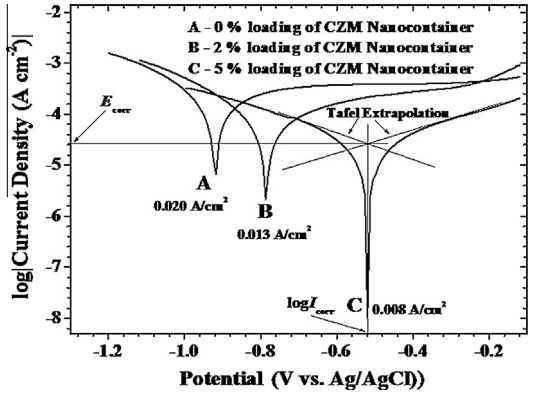

Fig. 10. Tafel plots of mild steel samples coated with different coating materials loaded with CZM nanocontainer in alkyd resin in 5 wt.% NaCl solution.

was carried out in 5 wt.% aqueous NaCl solution at room temperature. The Tafel plot is plotted as log (current density) as a function of applied potential (V vs. Ag/AgCl). The measured current density is generated from the corrosion process for any redox reactions (cathodic and anodic reactions) takes place simultaneously. The corrosion current density, I_{corr} and corrosion potential, E_{corr} values were found from the Tafel plot by Tafel extrapolation method. In this method tangents are drawn to anodic and cathodic curve and from its intersection corrosion current density, I_{corr} and corrosion potential, E_{corr} was estimated. The Tafel plot (E as a function of log ($|I|$), where I represents the total measured current density, i.e., $I_c + I_a$) can isolate these two cathodic and anodic reactions. It is established that corrosion current density was decreased from 0.02 (for neat alkyd resin) to 0.013 A/cm^2, when 2 wt.% CZM nanocontainers are dispersed in neat alkyd resin coatings and it is further decreased to 0.008 A/cm^2 when loading of CZM nanocontainers is increased to 5 wt.%. E_{corr} values are found to be shifted to the positive side from −0.917 to −0.519 V vs. Ag/AgCl with the addition of 5 wt.% of CZM nanocontainers in alkyd resin.

The overall results of release rate, and electrochemical (Tafel plot) analysis indicates that the addition by 5 wt.% CZM nanocontainers in alkyd resin shows a significant enhancement in the corrosion inhibitive properties compared to neat alkyd resin.

4. Conclusion

In the present study successful preparation of CZM nanoparticles, encapsulation CZM nanoparticles in PANI layer and deposition of polyelectrolyte layers as well as corrosion inhibitor (imidazole) for the preparation of CZM nanocontainers was carried out in the presence of ultrasonic irradiations. The principal conclusions are:

1. The presence of ultrasonic irradiation can accelerate the nucleation rate resulting in reduction of CZM nanoparticles size and which was found to be 26 nm. TEM images confirm the formation of smaller sized CZM nanocontainers, which is essentially due to the cavitational effects of ultrasonic irradiations during the preparation process.
2. The quantitative analysis of release of corrosion inhibitor i.e. imidazole from CZM nanocontainers was successfully carried out using different kinetic models like zero order, first order, Hixson–Crowell, Higuchi and Korsmeyer–Peppas models.
3. Results of release study, and electrochemical corrosion (Tafel plots) analysis of nanocontainer coatings on mild steel (MS) panel showed significant improvement in the anticorrosion performance of the nanocontainer/alkyd resin coatings, which is attributed to the optimum loading of the CZM nanocontainers.

Acknowledgments

S.H. Sonawane acknowledges the DRDO (Govt. of India) for providing the funding under the grant number ERIP/ER/1206027/M/01.

References

[1] A. Kalendova, D. Vesely, J. Gojny, K. Raskova, Development in the efficiency of anticorrosive pigments, in: Conference Papers of 35th Internationale Conference on Coatings Technology, 2004, pp. 141–151.
[2] V. Barranco, S. Feliu Jr., S. Feliu, EIS study of the corrosion behaviour of zinc-based coatings on steel in quiescent 3% NaCl solution, Corros. Sci. 46 (2004) 2203–2220.
[3] D.E. Walker, G.D. Wilcox, Molybdate based conversion coatings fro zinc and zinc alloy surfaces: a review, Trans. Inst. Met. Finish. 86 (2008) 251–259.
[4] D.G. Shchukin, H. Möhwald, Surface-engineered nanocontainers for entrapment of corrosion, Adv. Funct. Mater. 17 (2007) 1451–1458.
[5] A. Schlachter, M.E. Gruner, M. Spasova, M. Farle, P. Entel, Preparation and properties of nanostructured magnetic hollow microspheres: experiment and simulation, Phase Transit. 78 (2005) 741–750.
[6] T. Lopez, J. Sotelo, J. Navarrete, J.A. Ascencio, Synthesis of TiO_2 nanostructured reservoir with temozolomide: structural evolution of the occluded drug, Opt. Mater. 29 (2006) 88–94.
[7] D. Zhan, L. Qi, J. Ma, H. Cheng, Synthesis of submicrometer-sized hollow silver spheres in mixed polymer–surfactant solutions, Adv. Mater. 14 (2002) 1499–1502.
[8] G.S. Pappas, P. Liatsi, I.A. Kartsonakis, I. Danilidis, G. Kordas, Synthesis and characterization of new SiO_2–CaO hollow nanospheres by sol–gel method: bioactivity of the new system, J. Non-Cryst. Solids 354 (2008) 755–760.
[9] S.H. Sonawane, B.A. Bhanvase, A.A. Jamali, S.K. Dubey, S.S. Kale, D.V. Pinjari, A.B. Pandit, Improved active anticorrosion coatings using layer-by-layer assembled ZnO nanocontainers with benzotriazole, Chem. Eng. J. 189–190 (2012) 464–472.
[10] B.A. Bhanvase, Y. Kutbuddin, R.N. Borse, N. Selokar, D.V. Pinjari, S.H. Sonawane, A.B. Pandit, Ultrasound assisted intensification of calcium zinc phosphate pigment synthesis and its nanocontainer for active anticorrosion coatings, Chem. Eng. J. 231 (2013) 345–354.
[11] M.A. Patel, B.A. Bhanvase, S.H. Sonawane, Production of cerium zinc molybdate nano pigment by innovative ultrasound-assisted approach, Ultrason. Sonochem. 20 (2013) 906–913.
[12] H. Mingzhao, E. Forssberg, Y. Wang, Y. Han, Ultrasonication-assisted synthesis of calcium carbonate nanoparticles, Chem. Eng. Commun. 192 (2005) 1468–1481.
[13] M.L. Zheludkevich, D.G. Shchukin, K.A. Yasakau, H. Mohwald, M.G.S. Ferreira, Anticorrosion coatings with self-healing effect based on nanocontainers impregnated with corrosion inhibitor, Chem. Mater. 19 (2007) 402–411.
[14] F. Ghadimi, K. Dindar Safa, B. Massoumi, A. Akbar Entezami, Polyaniline doped with sulphosalicylic, salicylic and citric acid in solution and solid-state, Iran. Polym. J. 11 (2002) 159–166.
[15] B.A. Bhanvase, S.H. Sonawane, New approach for simultaneous enhancement of anticorrosive and mechanical properties of coatings: application of water repellent nano $CaCO_3$-PANI emulsion nanocomposite in alkyd resin, Chem. Eng. J. 156 (2010) 177–183.
[16] I.A. Kartsonakis, E.P. Koumoulos, A.C. Balaskas, G.S. Pappas, C.A. Charitidis, G.C. Kordas, Hybrid organic–inorganic multilayer coatings including nanocontainers for corrosion protection of metal alloys, Corros. Sci. 57 (2012) 56–66.
[17] I.A. Kartsonakis, A.C. Balaskas, E.P. Koumoulos, C.A. Charitidis, G.C. Kordas, Incorporation of ceramic nanocontainers into epoxy coatings for the corrosion protection of hot dip galvanized steel, Corros. Sci. 57 (2012) 30–41.
[18] I.A. Kartsonakis, E. Athanasopoulou, D. Snihirova, B. Martins, M.A. Koklioti, M.F. Montemor, G. Kordas, C.A. Charitidis, Multifunctional epoxy coatings combining a mixture of traps and inhibitor loaded nanocontainers for corrosion protection of AA2024-T3, Corros. Sci. 85 (2014) 147–159.
[19] M. Saremi, M. Yeganeh, Application of mesoporous silica nanocontainers as smart host of corrosion inhibitor in polypyrrole coatings, Corros. Sci. 86 (2014) 159–170.
[20] D. Suvakanta, P. Murthy, L. Nath, P. Chowdhury, Kinetic modeling on drug release from controlled drug delivery systems, Acta Pol. Pharm. Drug Res. 67 (2010) 217–223.
[21] B. Narsimhan, S. Mallapragada, N. Peppas, in: E. Mathiowitz (Ed.), Release Kinetics, Data Interpretation, Encyclopedia of Controlled Drug Delivery, John Wiley & Sons, 1999, pp. 921–935.
[22] T. Higuchi, Mechanism of sustained-action medication: theoretical analysis of rate of release of solid drug dispersed in solid, matrices, J. Pharm. Sci. 52 (1963) 1145–1149.
[23] B. Hixson, W. Crowell, Dependence of reaction velocity upon surface and agitation I—theoretical consideration, Ind. Eng. Chem. 23 (1931) 923–931.
[24] L. Chen, J. Zhu, B. Cheng, Preparation and in vitro evaluation of a novel combined multiparticulate delayed-onset sustained-release formulation of diltiazem hydrochloride, Pharma 62 (2007) 907–913.
[25] R. Korsmeyer, R. Gurny, E. Doelker, P. Buri, N. Peppas, Mechanisms of solute release from porous hydrophilic polymers, Int. J. Pharm. 15 (1983) 25–35.
[26] M. Tyagi, B.A. Bhanvase, S.L. Pandharipande, Computational studies on release of corrosion inhibitor from layer-by-layer assembled silica nanocontainer, Ind. Eng. Chem. Res. 53 (2014) 9764–9771.
[27] G.M. Treacy, G.D. Wilcox, M.O.W. Richardson, Behaviour of molybdate-passivated zinc coated steel exposed to corrosive chloride environments, J. Appl. Electrochem. 29 (1999) 647–654.
[28] M.F. Montemor, D.V. Snihirova, M.G. Taryba, S.V. Lamaka, I.A. Kartsonakis, A.C. Balaskas, G.C. Kordas, J. Tedim, A. Kuznetsova, M.L. Zheludkevich, M.C.S. Ferreira, Evaluation of self-healing ability in protective coatings modified with combinations of layered double hydroxides and cerium molibdate nanocontainers filled with corrosion inhibitors, Electrochim. Acta 60 (2012) 31–40.
[29] S. Ding, M. Wang, Studies on synthesis and mechanism of nano-$CaZn_2(PO_4)_2$ by chemical precipitation, Dyes Pigm. 76 (2008) 94–96.
[30] I.A. Kartsonakis, A.C. Balaskas, G.C. Kordas, Influence of cerium molybdate containers on the corrosion performance of epoxy coated aluminium alloys 2024-T3, Corros. Sci. 53 (2011) 3771–3779.
[31] T. Yousefi, A.R. Khanchi, S.J. Ahmadi, M.K. Rofouei, R. Yavari, R. Davarkhah, B. Myanji, Cerium(III) molybdate nanoparticles – synthesis, characterization and radionuclides adsorption studies, J. Hazard. Mater. 215–216 (2012) 266–271.
[32] I.A. Kartsonakis, G. Kordasw, Synthesis and characterization of cerium molybdate nanocontainers and their inhibitor complexes, J. Am. Ceram. Soc. 93 (2010) 65–73.
[33] A. Nilchi, B. Maalek, A. Khanchi, M. Ghanadi Maragheh, A. Bagheri, Cerium (IV) molybdate cation exchanger: synthesis, properties and ion separation capabilities, Radiat. Phys. Chem. 75 (2006) 301–308.
[34] Y. Sun, A.G. Macdiarmid, A.J. Epstein, Polyaniline: synthesis and characterization of pernigraniline base, J. Chem. Soc., Chem. Commun. 7 (1990) 529–531.
[35] A. Barth, Review: the infrared absorption of amino acid side chains, Prog. Biophys. Mol. Biol. 74 (2000) 141–173.
[36] X. Lu, Y. Yu, L. Chen, H. Mao, L. Wang, W. Zhang, Y. Wei, Poly(acrylic acid)-guided synthesis of helical polyaniline microwires, Polymer 46 (2005) 5329–5333.
[37] O. Lupan, L. Chow, G. Chai, H. Heinrich, Fabrication and characterization of Zn–ZnO core–shell microspheres from nanorods, Chem. Phys. Lett. 465 (2008) 249–253.
[38] T. Masui, H. Hirai, R. Hamada, N. Imanaka, G. Adachi, T. Sakata, H. Mori, Synthesis and characterization of cerium oxide nanoparticles coated with turbostratic boron nitride, J. Mater. Chem. 13 (2003) 622–627.
[39] R.S. Patil, M.D. Uplane, P.S. Patil, Electrosynthesis of electrochromic molybdenum oxide thin films with rod-like features, Int. J. Electrochem. Sci. 3 (2008) 259–265.
[40] I. Kartsonakis, I. Daniilidis, G. Kordas, Encapsulation of the corrosion inhibitor 8-hydroxyquinoline into ceria nanocontainers, J. Sol–Gel Sci. Technol. 48 (2008) 24–31.
[41] P. Matheswaran, A.K. Ramasamy, Influence of benzotriazole on corrosion inhibition of mild steel in citric acid medium, J. Chem. 7 (2010) 1090–1094.
[42] S.T. Selvi, V. Raman, N. Rajendran, Corrosion inhibition of mild steel by benzotriazole derivatives in acidic medium, J. Appl. Electrochem. 33 (2003) 1175–1182.
[43] A. Popova, M. Christov, Evaluation of impedance measurements on mild steel corrosion in acid media in the presence of heterocyclic compounds, Corros. Sci. 48 (2006) 3208–3221.
[44] P.G. Cao, J.L. Yao, J.W. Zheng, R.A. Gu, Z.Q. Tian, Comparative study of inhibition effects of benzotriazole for metals in neutral solutions as observed with surface enhanced Raman spectroscopy, Langmuir 18 (2002) 100–104.
[45] S. Ramesh, S. Rajeswari, Corrosion inhibition of mild steel in neutral aqueous solution by new triazole derivatives, Electrochim. Acta 49 (2004) 811–820.
[46] J. Siepmann, N.A. Peppas, Modeling of drug release from delivery systems based on hydroxypropyl methylcellulose (HPMC), Adv. Drug Deliv. Rev. 48 (2001) 139–157.
[47] P.L. Ritger, N.A. Peppas, A simple equation for description of solute release II. Fickian and anomalous release from swellable devices, J. Control. Rel. 5 (1987) 37–42.